ELSEVIER

The Effects of Forced Boundary Conditions on Flow Within a Cubic Cavity Using Digital Particle Image Thermometry and Velocimetry (DPITV)

Dana Dabiri
Mory Gharib
California Institute of Technology, Pasadena, California

■ Buoyancy-driven convection within a cavity, whose sidewalls are heated and cooled, is a problem of great interest, because it has applications in heat transfer and mixing. Most studies to date have studied one of two cases: the steady-state case or the development of the transient flow as it approaches steady state. Our main concern was to study the response of the cavity to time-varying thermal boundary conditions. We therefore decided to observe the flow phenomena within a convection cavity under sinusoidal thermal forcing of the sidewalls. To map the flow properly, it is necessary to have simultaneous kinematic and thermal information. Therefore, the digital particle image thermometry and velocimetry (DPITV) is used to acquire data. Implementing this technique requires seeding the flow with encapsulated liquid crystal particles and illuminating a cross section of the flow with a sheet of white light. Extraction of the thermal and kinematic content is in two parts. For the first, the liquid crystals will reflect different colors of the visible spectrum, depending on the temperatures to which they are subjected. Therefore, calibrating their color reflection with temperature allows for the extraction of the thermal content. For the second part, the kinematic information is obtained through the use of a digital cross-correlation particle image velocimetry technique. With the use of DPITV, the flow within a convection cavity is mapped and studied under steady forcing and sinusoidally forced boundary conditions at the Brunt-Väisälä frequency. For the sinusoidally forced case, three cases are studied. In the first, the heating between the two walls is in phase. In the second, the heating between the two walls is 180° out of phase. In the third, the heating between the two walls is 90° out of phase. For steady forcing, the thermal plots show that the flow develops a linearly stratified profile within the center of the cell. At the sidewalls, however, owing to forcing, hot/cold thermal boundary layers develop at the left/right walls. These hot/cold thermal boundary layers then turn around the upper-left/lower-right corners and develop into intrusion layers that extend across the top and bottom walls. The vorticity and streamlines show that the bulk of the fluid motion is concentrated around the walls, whereas the fluid within the center of the cell remains stationary. For the sinusoidally forced cases, the thermal plots show the existence of many thermal "islands," or pockets of fluid where the temperature is different with respect to its surroundings. The vorticity plots show that the center of the cell is mostly devoid of vorticity and that the vorticity is mainly confined to the sidewalls, with some vorticity at the top and bottom walls. For the 0° forcing, the streamlines show the development of two counterrotating rollers. For the 180° forcing,

Address correspondence to Dana Dabiri, Graduate Aeronautical Laboratories, California Institute of Technology, Pasadena, CA 91125.

Experimental Thermal and Fluid Science 1996; 13:349–363

655 Avenue of the Americas, New York, NY 10010

0894-1777/96/$15.00
PII S0894-1777(96)00113-6

the streamlines show the development of only one roller. Finally, for the 90° forcing, the streamlines show the development of both a two-roller and a one-roller system, depending on the position within the forcing cycle.

Keywords: *PIV, liquid crystal, thermometry, buoyancy, Rayleigh number, Prandtl number, Brunt-Väisälä frequency, natural convection, cavity*

INTRODUCTION

Most of the fluid flows that we are familiar with and come in daily contact with are flows that are induced by buoyancy. These include flows that occur in celestial bodies, in the oceans, and in the atmosphere—to name but a few. These buoyancy forces arise from density differences in the fluid of interest, usually brought about by temperature variations within the flow. It is important to note, however, that these types of flows, though similar, are different from momentum-driven fluid flows generated through any type of forcing, such as a pump or a fan. In the buoyancy-driven flows, for example, the temperature fields and the flow fields are always coupled. Also, little is known a priori about the naturally convected flow when compared with its momentum-driven counterpart.

Therefore, buoyancy-driven convection has developed into a problem of great importance not only because of its existence in nature, which affects us in all aspects of life, but because of its practical applications to heat transfer and heat-transport problems. Basically, buoyancy-driven flows can be classified into one of two areas: external flows and internal flows, although one can think of many combined or "mixed" problems. The internal flow problems have not been studied as extensively as the external flow problem, because they are quite complex. For example, in external flows, it is common to decouple the analyses of the viscous and thermal boundary layers from the very large ambient potential flow. However, in internal flows, the viscous and thermal boundary analyses cannot be decoupled from the finite-sized potential flow. In the former case, the ambient potential flow properties are always given as constant values for all times. But the ambient potential flow parameters for the latter case are given only as initial conditions, because they vary according to the behaviors of the viscous and thermal boundary layers.

There have been a variety of studies regarding cavity flows. One of the earliest to investigate flow confined to within a cavity was Batchelor [1], who analytically showed that, for $Ra < 1000$ and large aspect ratios, the heat-transfer mode is dominated by conduction. Gill [2], however, showed that, for a fixed large aspect ratio and large Rayleigh numbers, the flow was driven by the boundary-layer regions of the flow, where convection dominated the heat-transfer mode while the interior region remained stagnant and vertically stratified. The flow and temperature fields were perhaps best seen by Eckert and Carlson [3] for the different flow regimes.

The unsteady transient problem evolving into the steady state received little attention until Patterson and Imberger [4] (henceforth referred to as PI) initially approached the problem. Neglecting viscous dissipation, assuming two-dimensional flow, and calling on a series of scaling arguments, PI were able to show that there are six different approaches to steady state based on the initial parameters of the problem. A summary of their results is as follows:

1. In regime 1, where $Ra < 1$, the approach to steady state is dominated by pure conduction as expressed by Batchelor [1].
2. In regime 2, where $1 < Ra < \sigma^2$, the approach to steady state is by a combination of conduction and convection.
3. In regime 3, where $\sigma^2 < Ra < \sigma^4 A^{-4}$, where A is the aspect ratio defined as the height divided by the width, the approach to steady state is by convection. It was observed by PI that, in this approach, a vertical temperature gradient is generated through a continual horizontal layering of viscous fluid referred to as the viscous intrusion layer. However, the inertia of the boundary-layer flow owing to buoyancy is not sufficient to generate internal waves, as there will be for higher values of Ra.
4. In regime 4, where $\sigma^4 A^{-4} < Ra < \sigma^{10}$, the inertia of the boundary layer is higher than that of regime 3, causing internal waves to be generated and transmitted through the core of the square cavity. These waves are seen by observing the local value of Nusselt number at the center of the cavity over time.
5. In regime 5, where $\sigma^{10} < Ra < \sigma^{16} A^{-12}$, the approach to steady state is identical with regime 4; however, the inertia of the thermal boundary layer is so great that the resulting intrusion layers are dominated not by viscous forces anymore but by inertial forces. However, before this inertia-dominated intrusion layer reaches the far wall, it becomes viscous.
6. Finally, in regime 6, where $\sigma^{16} A^{-12} < Ra$, the inertia of the sidewall boundary layer is so great that the resulting horizontal intrusion layers remain inertial until they hit the opposite wall.

Again, it is important to note that, for regimes 4 through 6, the flow is convection dominated and that the internal wave motion is present. PI also observed the existence of a cavity-scale internal seiche. This, they suggested, was produced by the tilting of isotherms as a result of the cold and hot intrusion layers ejecting from the vertical wall boundary layers traveling across the cavity and finally spreading to match the entrainment into the opposite vertical wall. Owing to buoyancy forces, the tilted isotherms would then readjust, thereby creating a large time-scale oscillation that was on the order of the Brunt-Väisälä frequency.

In 1984, Ivey [5] conducted an experiment, using various mixtures of glycerol and water within a cavity with $A = 1$ to verify the existence of the cavity-scale oscillations. The Prandtl numbers and Rayleigh numbers used were $\sigma = 82$,

$Ra = 3.9*10^8$; $\sigma = 7.1$, $Ra = 9.2*10^8$; and, $\sigma = 6.6$, $Ra = 1.2*10^9$, placing the experiment within PI's regime 5. In fact, Ivey found inertial intrusion layers. However, he found that, when the boundary layer turned the vertical wall into the horizontal wall, the boundary layer, now termed intrusion layer, suddenly thickened as it traveled across the horizontal adiabatic wall. This, he believed, was the result of the intrusion layer going through a hydraulic jump.

In 1989, Schladow *et al.* [6] revisited the problem to obtain further insights brought about from questions raised by Ivey. Two-dimensional and three-dimensional simulations were done for $Ra = 2*10^9$, $A = 1$, and $\sigma = 7.1$. Several interesting phenomena were shown. First, the three-dimensional center-plane calculations showed little difference between it and the two-dimensional flow. Second, simulations involving nonadiabatic conditions at the top and bottom walls showed that the effect of transient flow was insignificant, and the kinematics were virtually identical with the insulating case. Third, the scaling laws given by PI, especially the oscillatory approach to steady state, were shown to be correct. Finally, as was shown by Ivey, Schladow numerically confirmed that the horizontal intrusion layer showed a sudden expansion in width, which was not understood by the authors at the time.

Hiller *et al.* [7, 8] performed experimental and numerical work within a cube, where Ra ranged from 10^4 to 10^6, σ ranged from 200 to 6900, and ΔT between the two sidewalls ranged from 2.5°C to 18°C. Their results showed that the flow structure away from the vertical midplane of the cavity is strongly three-dimensional. They also found that, as the Ra was increased, the streamlines developed from a single spiral, starting at both the nonheated sidewalls and moving toward the midplane, into a double spiral configuration, where two adjacent spirals start at the nonheated sidewalls and move toward the midplane.

Patterson and Armfield [9] conducted both numerical and experimental experiments to fully understand the formation of the intrusion flow structures and the oscillations in the Nusselt number. The main parameters were $\sigma = 7.5$, $Ra = 3.26*10^8$, and $A = 1$. An explanation was given for the sudden expansion of the intrusion layer. The thermal boundary layer, upon exiting the vertical wall, has all the characteristics of a thermal boundary layer. However, upon turning the corner and becoming horizontal, it must satisfy the adiabatic boundary condition at the horizontal wall. Thus, because heat cannot exit through the wall, heat must be transferred through the fluid into the cavity. Thus, temperature decreases closest to the wall while increasing more toward the interior of the cavity. Thus, the intrusion layer will be blocked by the cooler fluid and forced to move around it. Because the intrusion layer is inertial, it behaves like a jet until its momentum decays and the flow is dominated by viscosity. In this case, buoyancy and conduction then allow the fluid to spread back onto the horizontal walls.

To resolve the difference between experimental and numerical observations, Schladow [10] performed several numerical simulations. For $Ra = 2*10^8$, $A = 1$, and $\sigma = 7.1$, Schladow was able to show that long-period oscillations exist and are the result of the tilting of the isotherms. The frequency and amplitude of these oscillations were found to be in close agreement with those measured by Ivey. The explanation of the flow phenomena referred to earlier as an internal hydraulic jump, was found to be incorrect.

Lastly and most recently, Tong and Koster [11] have numerically studied two-dimensional flow within a rectangular cavity, using a non-Boussinesq parabolic density-temperature relation. In this study, they show the variation of the flow characteristics, such as the streamlines and the temperature contours, as a function of the Rayleigh number and the cell's aspect ratio.

Objective

All studies until now have focused on understanding the physics associated with transient natural convective flow within a square cavity approaching steady state. However, as far as the authors are aware, no attempt has been made to study the flow under sinusoidally forced boundary conditions for this geometry. PI suggest that, for the transient case, the spreading of the intrusion layers cause "a tilting of the isotherms beyond the horizontal and the consequent generation of internal waves of frequency $O(\omega)$,

$$w \sim \frac{N}{(1 + A^2)^{1/2}}, \tag{1}$$

where the Brunt-Väisälä frequency is defined by $N \sim (\upsilon k Ra)^{1/2}/h^2$," where A, υ, k, Ra, and h are the aspect ratio of the cell, kinematic viscosity, thermal diffusivity, Rayleigh number, and the height of the cell, respectively. Therefore, the oscillations seen are at the order of the Brunt-Väisälä frequency, corrected by a factor that incorporates the aspect ratio of the cell.

It is therefore of interest to map the flow patterns, vorticity fields, and temperature fields by heating and cooling the opposite walls sinusoidally at 0°, 90°, and 180° at this oscillation frequency to study the fluid's behavior. However, to provide a base case for which comparisons can be referred, the steady-state fluid behavior within a square cavity, where one sidewall is continuously heated while the opposite sidewall is cooled, will be mapped and studied as well.

MEASUREMENT TECHNIQUE, EXPERIMENTAL FACILITIES, AND SETUP

Digital Particle Image Thermometry and Velocimetry (DPITV)

All experimental work mentioned here to fore has been done with single point measurement probes. However, owing to the unsteady nature of this flow, it is desirable to use a two-dimensional technique capable of providing both thermal and kinematic results. To study the fluid flow within the convection cell, it is important to be able to measure and map the velocity and temperature simultaneously within a two-dimensional cross-section midplane of the convection cell. The technique used to measure temperature and velocity is a combination of the digital particle image thermometry (DPIT) and digital particle image velocimetry (DPIV) techniques, referred to as the DPITV technique [12]. This technique requires that the flow be seeded with liquid crystal particles that will act as the temperature and velocity sensors. A cross section of

the desired flow is then illuminated with a white light sheet. Upon illumination, the liquid crystal particles will reflect different colors, depending on the different temperatures to which they are subjected. The reflected colors are then captured with a Sony XC-007 three-chip color camera for correct color acquisition and stored on a Sony 5000A LVR/LVS laser video disk storage system at a 512×480 pixel^2 resolution (Fig. 1). For analysis, the colors are analyzed within the HSI (hue, saturation, and intensity) color space. The spectral content of the color, which characterizes temperature, is contained within the hue parameter. Thus, the hue buffer is used to extract the thermal information. Further details on the measurement of temperature with liquid crystal particles can be found in Dabiri and Gharib [13]. To extract velocities, the intensity buffers of consecutive image pairs are processed sequentially. These buffers contain grey-scale information on the liquid crystal particle intensities. For each image pair, an interrogation window extracts a small part of the images (32×32 pixel^2 in pixel domain and 1.7×1.7 mm^2 in real domain) in the same location and performs a cross-correlation incorporating a Gaussian subpixel resolution of .01 pixel, resulting in an average shift of liquid crystal particles for that window. This interrogation window is then systematically incremented through the whole image, producing a two-dimensional vector domain [14].

Previous work has also combined the use of liquid crystal thermometry and PIV techniques to provide simultaneous thermal and kinematic results. Kimura *et al.* [15] have used a single-chip CCD color camera to record the liquid crystal color reflections on a video tape recorder. Unfortunately, the use of a single-chip color camera as well as a video tape recorder did not allow for accurate color reproduction. Furthermore, their images were digitized at a lower resolution of 240×440 pixel^2. Moreover, the digital cross-correlating PIV technique that they used did not allow for subpixel measurement. Ozawa *et al.* [16] employed the techniques developed by Kimura *et al.* to study natural convection in a Hele-Shaw cell. However, their results also suffered from lack of subpixel measurement in their velocities and improper color reproduction in their temperature results.

Experimental Facility

Figures 2a–2c show a diagram of the experimental setup. As can be seen, the convection cell in which the experiment takes place is located within a larger ambient, constant-temperature bath. The convection cell is $2.54 \times 2.54 \times 2.54$ cm^3, where two opposing sidewalls are TECA thermoelectric heaters, the other two opposing sidewalls and the bottom wall are quartz glass, and the top wall is a Plexiglas cover. To ensure proper functioning of the thermoelectric heaters, their opposite sides must be kept at a constant temperature. Therefore, the temperature within the constant-temperature baths encasing the convection cell must be kept constant. To ensure that these baths remain at a constant temperature, a Neslab RTE-110 external constant temperature controller, with an accuracy of ± 0.1°C, is used to regulate the temperature of the fluid within the constant-temperature baths. To check the surface temperature variation of the thermoelectric heaters, thermocouples were mounted onto the surface of the thermoelectric heaters. To prevent obstruction of the flow by the bluntness of the thermocouples, the surface of the thermoelectric heaters was covered with a thin layer of

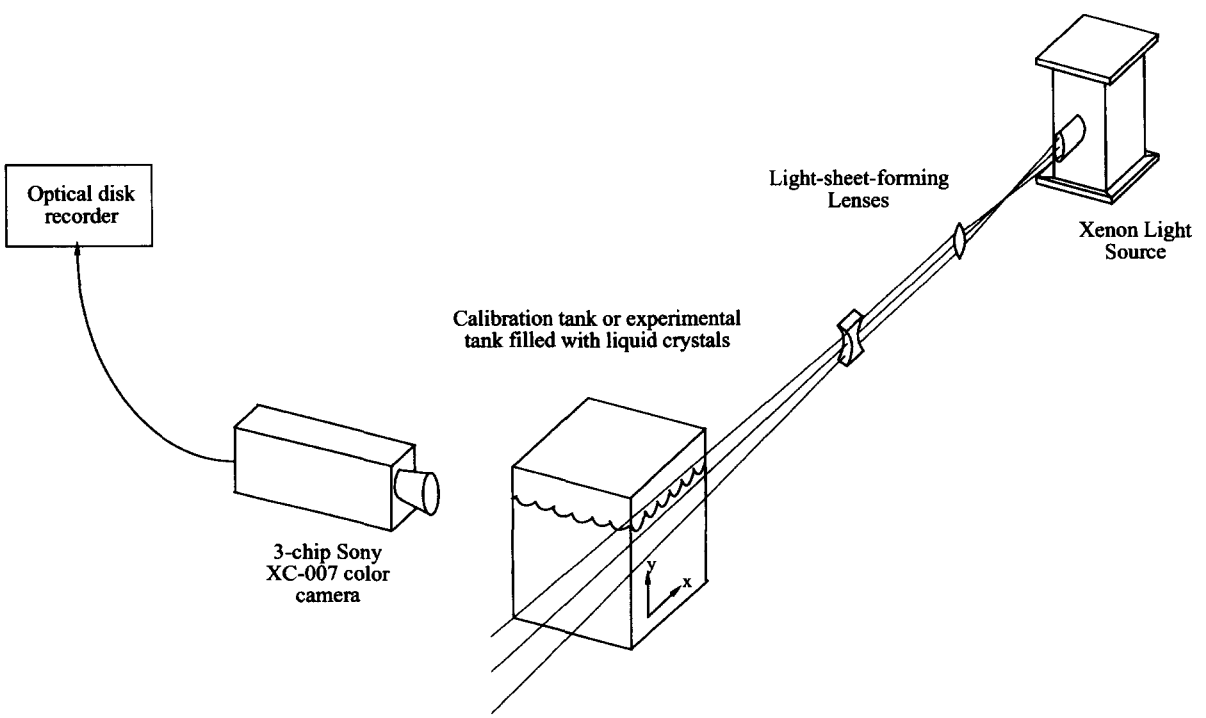

Figure 1. Setup for performing both the calibration and the experiment. The two-dimensional cross section of the center plane of the cell is illuminated with a sheet of white light generated from a Xenon arc-lamp while liquid crystal color reflections are captured by using the three-chip color camera and stored on the optical disk drive.

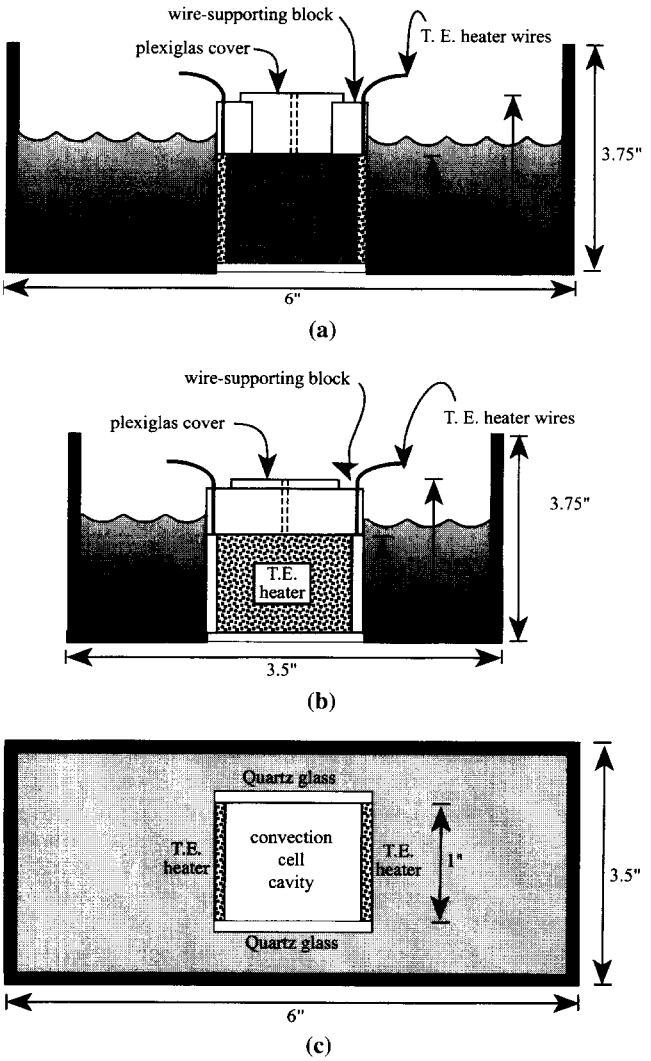

Figure 2. Convection cell: (a) side view (the bottom plate of the convection cell cavity is made of quartz glass); (b) front view (the bottom plate of the convection cell cavity is made of quartz glass); (c) top view (the wire-supporting blocks and the Plexiglas are not shown for better viewing purposes).

silicon RTV, such that the thermocouples were embedded within this layer. The thermocouples showed that the surface temperature was uniform to within 0.1°C. To isolate the cell from vibrations, the convection cell is mounted onto a three-point leveling system attached to a rigid frame. The center of this frame is left open to allow for illumination of the convection cell from below. To further reduce vibrations, the Neslab chiller as well as the function generators and amplifiers that drive the thermoelectric heaters are placed on separate tables apart from the convection cell and its frame.

Calibration Setup

The color reflection of the liquid crystal is dependent on the angle from which it is observed. Therefore, the calibration and the experiment are performed in the same experimental apparatus and with the same experimental setup. A 25% glycerol/water solution, seeded with encapsulated liquid crystal particles, is held within the convection cell explained in the next section. This mixture resulted in a calculated Prandtl number of 12.4. Liquid crystal particles (50 μm) are used to seed the flow. The liquid crystal particles' color response is from 21.9° to 26.1° centigrade. A Xenon short-arc lamp and a series of optics are used to create a sheet of white light 2-mm thick to illuminate the center-plane cross section of the convection cell. A three-chip CCD color camera (Sony XC-007) is used to capture the color reflection of the liquid crystal particles and store them on the Sony 5000A LVR/LVS laser disk recorder. The liquid crystal particle mixture is then heated to different constant temperatures to within $\pm 0.1°$, where, for each temperature, images are captured and hue values are recorded. After thresholding [10], hue values are collected from each of the calibration images and averaged for each image. The hue averages and standard deviations for each image are then plotted against their corresponding temperatures, and a second-order polynomial is used to curve-fit the data.

Experimental Setup and Data Analysis

As mentioned earlier, the experimental setup is identical with the calibration setup. The Xenon light sheet described in the preceding section is used to illuminate the center plane of the convection cell from below. A three-chip CCD Sony XC-007 color camera used for calibration is also used to capture the color reflections of the liquid crystal particles at 90° from the incident light sheet onto the laser disk recorders. The location of the three-chip color camera in the experimental setup is identical with its position in the calibration setup in terms of its distance to the setup, the focus of the lens, its zooming distance, its aperture opening, and most importantly, its viewing angle.

After data acquisition, the desired images are fed from the laser disk recorder into the P.C.-based DT-2871 image processing board frame by frame. After thresholding, the hue field for the region of interest within the particular frame is then translated into temperature through the calibration curves, thereby giving the temperature field.

To extract the velocity information, the intensity buffers of two frames with a known time difference between the two are initially chosen. The DPIV technique is then implemented on the intensity buffers, thereby producing the velocity field for that particular point in time. This process is then repeated for different times.

RESULTS

Calibration Results

The distance of the camera to the experiment is such that the viewing angle is 8°. There were two options for accommodating the varying hue throughout this viewing angle. The first option is to subdivide the calibration images and create local calibration curves for each of the subdivisions. Then, for extraction of temperature from the hue, depending on the location analyzed, the corresponding calibration curve is used. The second option is to use the whole of the calibration images and create a global calibration curve. After this, it is necessary to make a correction to the temperature reading to account for the angular

variations. Images are captured, where the temperature throughout each image is uniform. For each constant temperature, the acquired images are then averaged, thereby producing a global calibration curve that has averaged the artificial temperature variations due to angular variations.

For this report, a combination of both is used. First, a local calibration curve of hue versus temperature is calculated for the center of the cell. Second, images of the whole center plane of the cell are captured, where the fluid within the cell is at a constant temperature of 24°C. The spatial hue variations and corresponding artificial spatial temperature variations are then calculated. Finally, these two approaches are combined. The artificial temperature variation derived from the second approach is applied to the local calibration of the first approach to provide spatial corrections of the temperature measurements throughout the midplane due to varying viewing angles. The calibration of the hue values versus the temperature is shown in Fig. 3. The observed temperature range of the liquid crystal is 4°, ranging from 21.9°C to 26.1°C. The thermocouple temperature measurements were at an uncertainty of $\pm 0.1°$. The hue variations for each of these points are shown with the horizontal error bars. The vertical error bars represent the temperature errors due to the errors in the hue. Unfortunately, because these errors are quite large, only qualitative information can be extracted from the temperature plots. A second-order polynomial curve is fitted to the data. The correlation coefficient for this curve fit is .983.

For the DPIV analysis, the time separation between images was 33.33 ms. The digitized area is 512×480 pixels^2, which was processed with an interrogation window size of 32×32 pixels^2 and a step size of 16×16 pixels^2 (50% window overlap). The uncertainty in the velocity measurements is 0.3%.

Experimental Results

As mentioned in the introduction, four sets of experiments were conducted: (1) steady-state heating/cooling of the convection cell, (2) sinusoidal heating and cooling of the sidewalls at the Brunt-Väisälä frequency with 0° phase shift between the heating and cooling cycles of the two heaters, (3) sinusoidal heating and cooling of the sidewalls at the Brunt-Väisälä frequency with 90° phase shift between the heating and cooling cycles of the two heaters, and (4) sinusoidal heating and cooling of the sidewalls at the Brunt-Väisälä frequency with 180° phase shift between the heating and cooling cycles of the two heaters. Eleven equidistant points were chosen within each cycle, and their results will be presented. Figures 4a–4c show the position of each of the 11 points chosen within the cycle for each of the three experiments with phase shifts. The Brunt-Väisälä frequency is found by heating the sidewalls for a brief period and measuring the oscillation period that follows. With this method, the Brunt-Väisälä period is measured to be 25.9 s, and the distance between observed points within the cycle is 2.35 s. Interestingly, the frequency of oscillation calculated from Eq. (1) gives an oscillation period of 1.9 s. The difference between the measured oscillations and the calculated period is due to the fact that the present flow is three-dimensional, whereas the flow shown by PI is two-dimensional. The Rayleigh number for all the cases, based at the maximum temperature difference and the height of the convection cell, is 7.2×10^5. For all the oscillatory cases, the streamline, vorticity, and temperature were measured, calculated, and plotted for all the positions indicated in Figs. 4a–4c. However, only particular positions will be shown and discussed to demonstrate the main features of these flows. Thus, for all the cases, the streamline plots are on the right, and the vorticity plots, superimposed on the temperature distributions, are shown on the left of Figs. 5–12. In the vorticity and streamline plots, solid lines represent positive values and dashed lines represent negative values. The streamline values represent the value of the stream function. The temperature plots are shown in grey scale, where darker shades represent the colder temperatures and lighter shades represent the hotter temperatures.

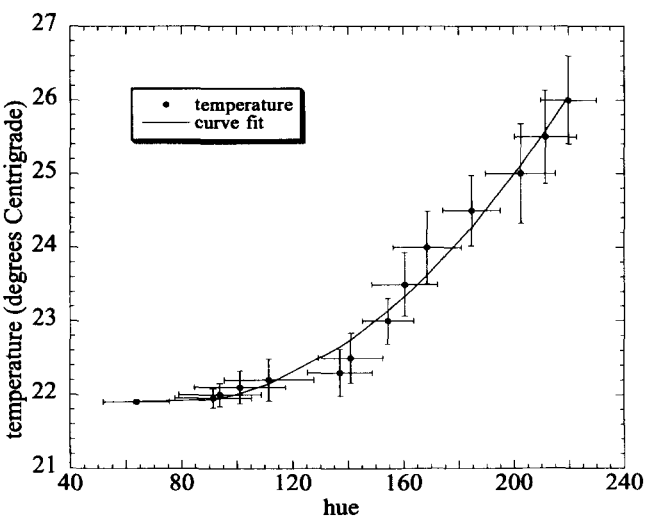

Figure 3. Calibration curve for the liquid crystal. The polynomial curve fit is $y = 22.985 - 0.029589 * x + 0.00019794 * x^2$.

Steady-State Heating / Cooling The streamlines shown at the right in Fig. 5 show that the flow velocity is strongest at the sidewalls, where the streamlines are closely spaced. Also seen is that the flow within the core is almost stationary. The streamlines are quite similar to those shown by Tong and Koster [9]. Of interest are their streamline plots for both $Ra = 10^5$ and $Ra = 10^6$. For $Ra = 10^5$, their streamlines show that, after the fluid flows vertically along the sidewall and turns around the corner, the horizontal streamlines slightly diverge and then converge again as they flow into the opposite corner. This situation is accentuated for their streamline plots of $Ra = 10^6$. Our case is at $Ra = 7.2 * 10^5$, and is therefore in between the two cases presented by the numerical work of Tong and Koster. Consequently, our streamlines exhibit the same behavior as that which Tong and Koster show for $Ra = 10^5$, yet not as pronounced as that shown for their $Ra = 10^6$ case. Interestingly, even though the present flow is three-dimensional, the flow within the center plane shows a two-dimensional behavior. The vorticity distribution in Fig. 5 shows that vorticity is concentrated mostly along the sidewalls. Likewise, because the core is almost stationary, as shown by the streamline plot, the

vorticity within the core is negligible with respect to that seen within the boundary layer. The vorticity plots also show that the vorticity levels associated with the intrusion layers on the top and bottom walls are much lower than those seen within the boundary layers. The temperature distribution in Fig. 5 shows that there is a fully developed hot/cold thermal boundary layer on the left/right wall. Note that the hot/cold thermal boundary layers, upon reaching the horizontal wall, turn the corner and proceed to flow as intrusion layers. As the flow approaches the opposite sidewall, the temperature changes accordingly, and the fluid entrains into the new thermal boundary layer. Because, at steady state, the core is relatively motionless, a thermal stratification develops through the core of the convection cell. The temperature distribution shows a region of closely spaced vertical isotherms near the sidewalls, with a sparse distribution of horizontal isotherms within the core. The vertical isotherms at the sidewalls turn around the top left and bottom right corners and become horizontal with respect to the top and bottom walls, respectively. However, these isotherms then turn into the wall and terminate almost perpendicular to these walls. This is much more evident on the bottom wall, indicating an adiabatic condition. However, the top wall does not show the same behavior as the bottom, indicating that this wall has not been made to satisfy the adiabatic condition as well as the bottom wall. However, as mentioned in the introduction, Shladow *et al.* [6] showed that nonadiabatic conditions at the top and bottom walls were virtually identical with the adiabatic case for transient flow. The behavior of the isotherms for the adiabatic case has in fact been calculated and predicted by the tempera-

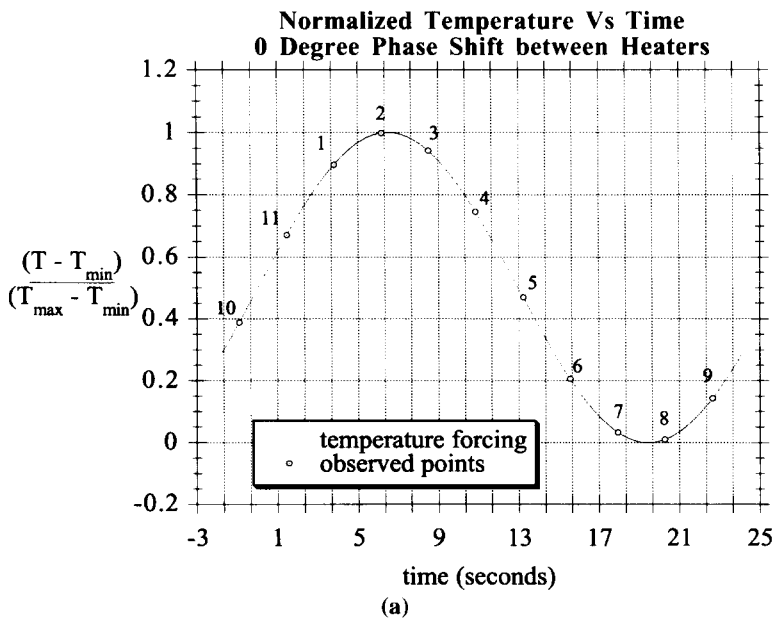

Figure 4. The sinusoidal wall temperature of the thermoelectric heaters for the (a) 0° phase-shift experiment (the positions in which data were collected are at −0.9, 1.45, 3.81, 6.16, 8.52, 10.87, 13.22, 15.58, 17.94, 20.20, and 22.65 s); (b) 180° phase-shift experiment (the positions in which data were collected are at −0.22, 2.15, 4.49, 6.86, 9.20, 11.54, 13.91, 16.25, 18.59, 20.96, and 23.30 s); (c) 90° phase-shift experiment (the positions in which data were collected are at −1.77, 0.58, 2.94, 5.29, 7.65, 10.00, 12.35, 14.71, 17.07, 19.42, and 21.77 s).

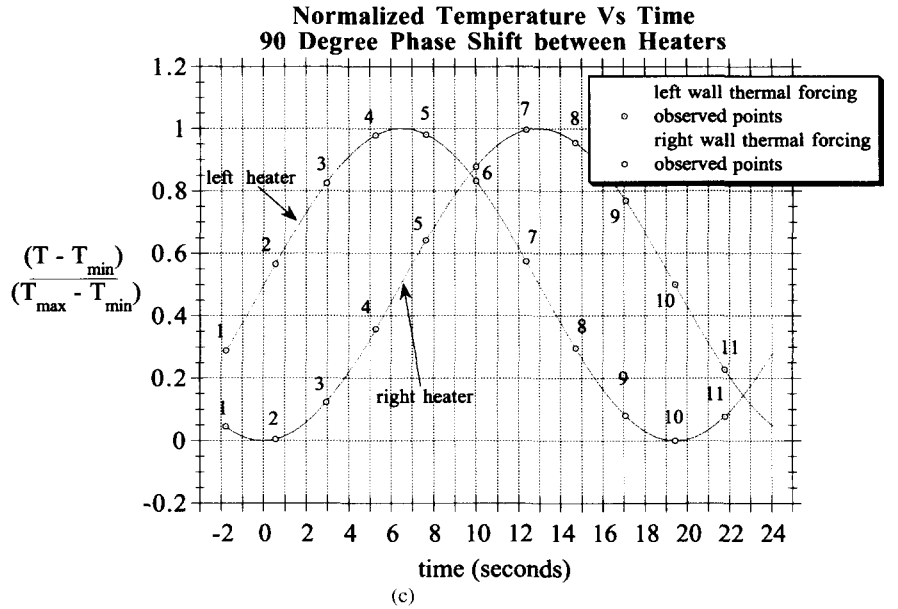

Figure 4. Continued

ture field calculations of Tong and Koster. Their calculations are consistent with the present findings. They show that, on the sidewalls, the isotherms are closely spaced owing to the thermal boundary layer on the sidewalls. Their results also show sparsely spaced horizontal isotherms within the core of the cell, indicating a linearly stratified temperature distribution throughout a stationary core.

Sinusoidal Heating with 0° Phase Shift Between Heaters

Figures 6 and 7 show the streamline, vorticity, and temperature distributions for this experiment at positions 2 and 5 within the cycle shown in Fig. 4a. For this flow, the fluid initially moves up both sidewalls as the sidewalls are heated and develops into two adjacent rollers, rolling in opposite directions (Fig. 6: position 2). As the heating cycle changes into a cooling cycle, the fluid changes direction and moves down both sidewalls, reducing its velocity (Fig. 7: position 5). As the cooling increases further, the flow develops into two adjacent rollers, as in the heating cycle, but rolling in the opposite direction. Note that position 2 corresponds to the position of maximum heating of the sidewalls, whereas position 5 corresponds to the position of midway transition from the strongest heating (position 2) to the strongest cooling (position 8). For this case, the temperature plots show many thermal "islands" compared with the steady-state case.

Position 2. The streamlines seen within Fig. 6 show that, at this position, owing to the strong heating of the side-

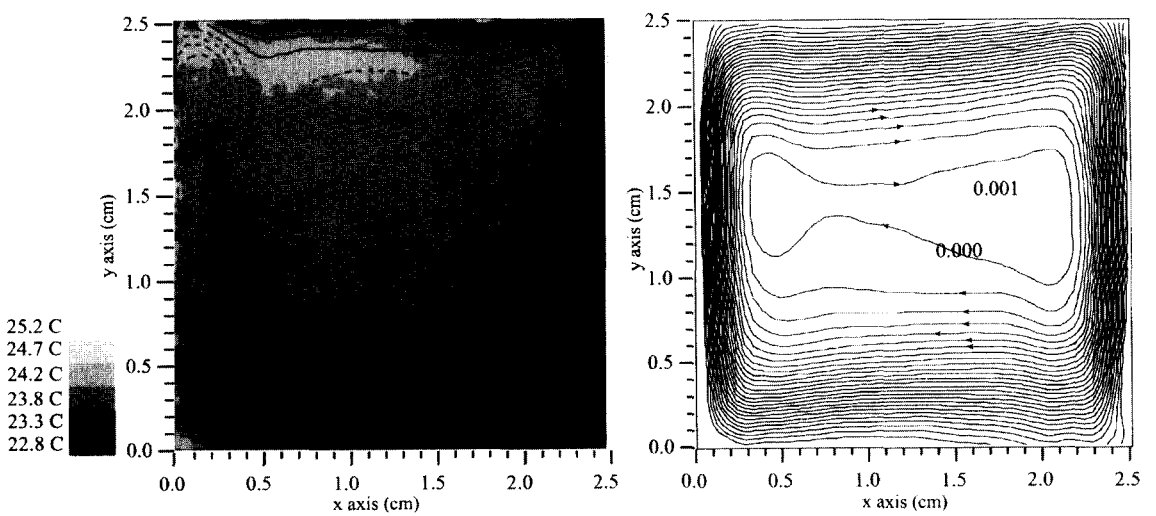

Figure 5. Steady-state case: the right plot is the streamline plot; the left is the vorticity plot superimposed over the temperature plot. The temperature, vorticity, and streamline contours are in increments of .485° centigrade, 0.05/s, and .001 m^2/s, respectively. The axes are in centimeters.

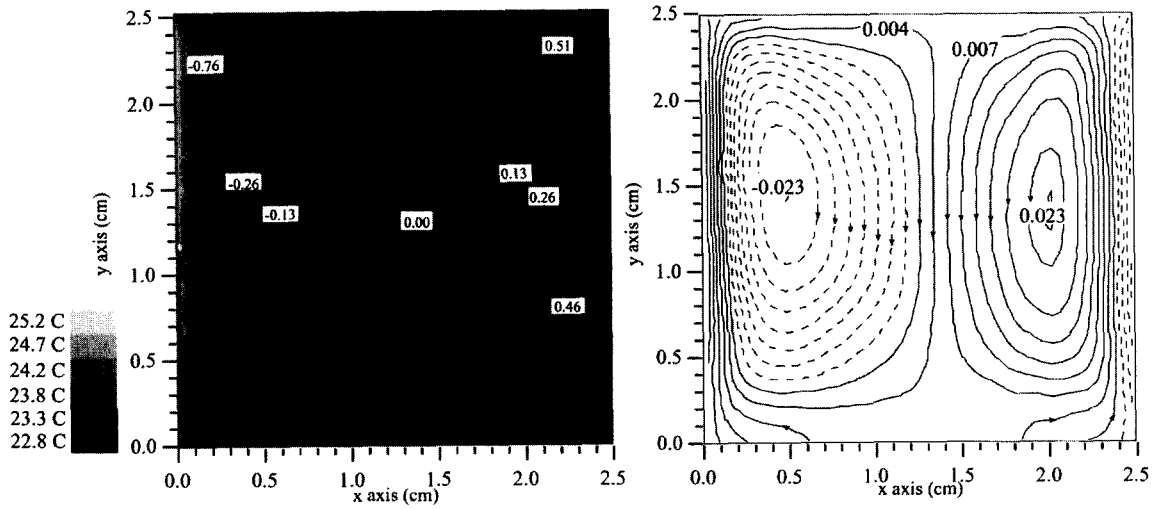

Figure 6. Position 2: 0° phase-shift. The right is the streamline plot, and the left is the vorticity plot superimposed over the temperature plot. The temperature, vorticity, and streamline contours are in increments of .485° centigrade, 0.128/s, and .003 m^2/s, respectively. The axes are in centimeters.

walls, the flow has developed into two strong counterrotating rollers situated side by side. The vorticity distribution shows that all the vorticity is concentrated along the sidewalls while the core of the fluid is devoid of vorticity. The streamlines toward the top/bottom wall are slightly tilted downward/upward from the corners toward the center of the cell. This indicates that, as the flow turns around the top corners onto the top wall, the top wall boundary layer thickens into the intrusion layer and, in doing so, reduces its vorticity level dramatically. The temperature field seen in Fig. 6 shows a fully developed thermal boundary layer on both sidewalls. Two cold spots are also seen in the lower corners that are left over from the previous cooling cycle's thermal boundary layers. Lastly, the streamlines show that, within the center plane, the two rollers are highly two-dimensional. The areas that exhibit three-dimensionality are at the midpoints of the top and bottom wall where the rollers meet. Here, the streamlines turn into the horizontal walls, indicating three-dimensional effects.

Position 5. The temperature field seen in Fig. 7 shows the development of the cold thermal boundary layers just inside the previous cycle's hot thermal boundary layer. The hot thermal layer left over from the previous cycle is seen to be convecting up the sidewalls and onto the top wall's intrusion layers. Finally, note that the small pockets of cold fluid seen at the previous position, which were remnants of the previous cycle's cold boundary layer, have now been entrained into the hot thermal boundary layer and have therefore reduced in size and temperature.

The streamlines show that the flow is moving slowly, because its contour values are changing mildly with respect to the previous position. It can then be concluded

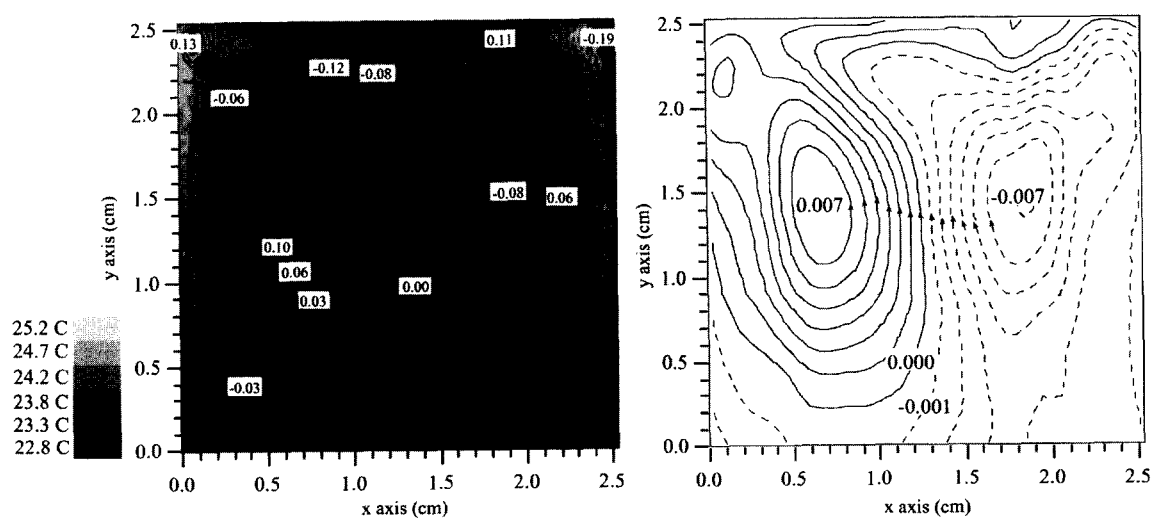

Figure 7. Position 5: 0° phase-shift. The right is the streamline plot, and the left is the vorticity plot superimposed over the temperature plot. The temperature, vorticity, and streamline contours are in increments of 0.485° centigrade, 0.032/s, and .001 m^2/s, respectively. The axes are in centimeters.

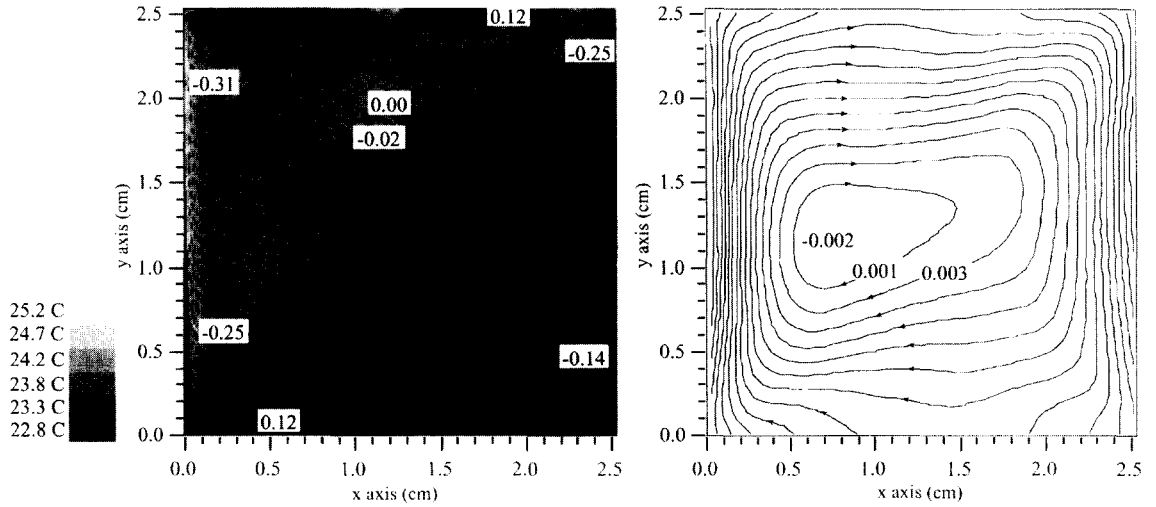

Figure 8. Position 8: 180° phase-shift. The right is the streamline plot, and the left is the vorticity plot superimposed over the temperature plot. The temperature, vorticity, and streamline contours are in increments of 0.485° centigrade, 0.03/s, and .002 m^2/s, respectively. The axes are in centimeters.

that the temperature is being distributed predominantly through conduction. The vorticity field shows a rich distribution of vorticity throughout the domain. Owing to the flow reversal that is beginning to occur, the vorticity that was generated at the sidewalls and had diffused inward is now amplified, pushing the negative/positive vorticity that had existed previously on the left/right sidewalls inward. The streamlines also show that the two central rollers do remain slightly two-dimensional, because some of the rollers' streamlines are closed. However, most of the flow at this position becomes three-dimensional, especially adjacent to all walls, because the streamlines terminate on the walls.

Sinusoidal Heating with 180° Phase Shift Between Heaters

Figures 8 and 9 show the streamline, vorticity, and temperature distributions for this experiment at positions 8 and 1 within the cycle shown in Fig. 4b. Because the heating of the sidewalls is 180° out of phase, the flow moves up the heated left wall and down the cooled right wall. This creates a central roller within the cell that rotates clockwise (Fig. 8: position 8). As the cycle reverses, the fluid flow along the sidewalls reverses, reducing the momentum of the central roller, such that the flow has very small velocities (Fig. 9: position 1). Note that position 8 corresponds to very high heating/cooling of the sidewalls, whereas position 1 corresponds to the transition from the strongest heating/cooling to the strongest cooling/heating. As in the previous case, there are many thermal "islands" compared with the steady-state case.

Position 8. The temperature field shows the full development of the thermal boundary layer. The streamline plots show that the flow is rotating in a clockwise direc-

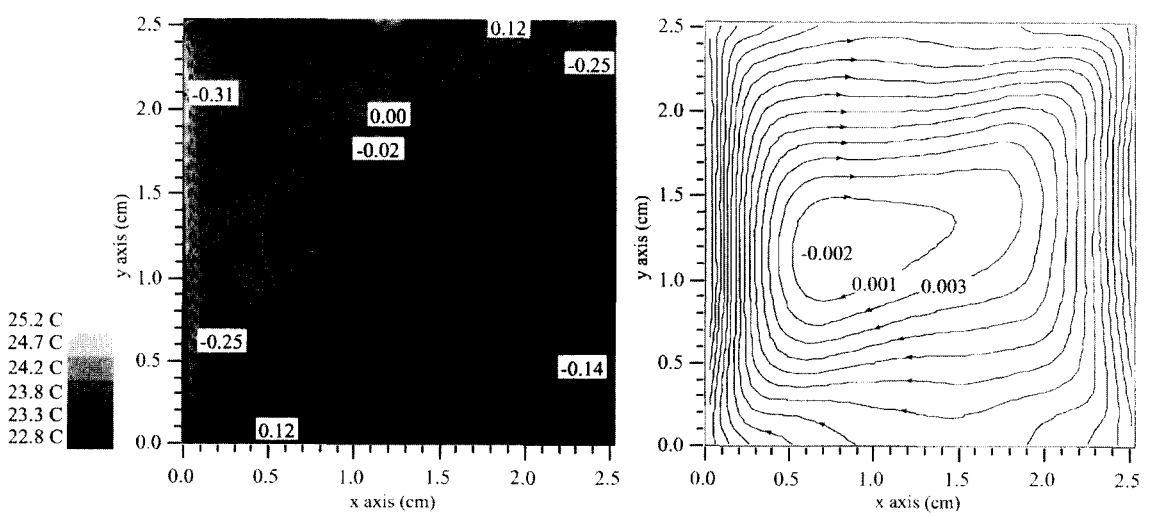

Figure 9. Position 1: 180° phase-shift. The right is the streamline plot, and the left is the vorticity plot superimposed over the temperature plot. The temperature, vorticity, and streamline contours are in increments of 0.485° centigrade, 0.04/s, for negative contours, .029/s for positive contours, and .002 m^2/s, respectively. The axes are in centimeters.

tion. The flow along the vertical walls shows a higher velocity than those along the horizontal walls, because the streamlines are spaced more closely at the sidewalls than at the horizontal walls. The streamlines confirm that the flow is rotating in one direction, creating a central roller within the center plane of the cell. It is interesting to note that the streamlines show an asymmetry, where the streamlines turn closer to the upper-right and lower-left corners than they do to the other two corners. This was also observed in the numerical results of the investigators mentioned in the introduction. This suggests that the origin of the thermal and viscous boundary layers entrains fluid from the core region into the origin of the boundary layers—in this case, the upper-right and lower-left corners rather than the adjacent walls. The streamlines also show that the flow at this position is strongly two-dimensional in the center plane, except at the horizontal walls, where the streamlines terminate at the walls. Lastly, note that the core is devoid of vorticity, as the flow has developed more fully, even though the temperature profiles show many thermal islands.

Position 1. The temperature plot seen in Fig. 9 shows the cold/hot thermal boundary layer on the left/right walls. The hot and cold thermal boundary layers turn their respective corners and deposit hot/cold fluid into the top-right/bottom-left intrusion layers, respectively. The flow has slowed down throughout the cell, as seen by larger contour spacing of the streamlines. The new thermal boundary layers are just developing. Therefore, because the velocities are small, heat transfer is mainly through conduction. The vorticity distribution shows two positive layers adjacent to the vertical walls. As the heating of the flow reverses on the sidewalls, the flow reverses direction as well, thereby generating these positive vorticity layers. The larger areas of negative vorticity directly adjacent to these two positive vorticity layers are the result of the previously generated thermal boundary layers seen in Fig. 8. Lastly, the streamlines show that, as the flow reverses at this position, though the center of the flow remains weakly two-dimensional, the rest of the flow is highly three-dimensional, as more of the streamlines terminate into all walls.

Sinusoidal Heating with 90° Phase Shift Between Heaters

Figures 10 through 12 show the streamline, vorticity, and temperature distributions for this experiment at positions 1, 2, and 4, respectively, within the cycle shown in Fig. 4c. The flow patterns seen here are a combination of the previous two cases. Because the heating of sidewalls is 90° out of phase, the right wall is fully cooling the flow, whereas the flow on the left wall is just beginning to reverse from cooling to heating. This creates a strong clockwise roller in the right half of the cell. Because the flow is almost beginning to reverse on the left wall, there is negligible flow on the left half of the center plane of the cell. At position 2, though the cooling on the right wall has increased, the flow has reversed as the left wall is being heated. This creates a central roller that is forced mainly from the right sidewall, because its cooling is stronger than the heating of the left wall. Lastly, position 4 shows the flow where there still exists a central roller. In this case, the roller within the cell also shows asymmetry. However, for this position, the left wall's heating is forcing its boundary layer more strongly than the right wall's cooling of its boundary layer. Note that positions 1 and 2 correspond to the position of near maximum cooling of the right sidewall and the beginning of heating of the left sidewall. Position 4 corresponds to the position of midway transition from the strongest cooling of the right sidewall (position 2) to the strongest heating of the right sidewall (position 7). It is important to notice that, for this case, there are many thermal "islands" compared with the steady-state case.

Position 1. The temperature field shown in Fig. 10 shows a hot thermal boundary developing on the left sidewall. Because the streamlines for the left wall show small

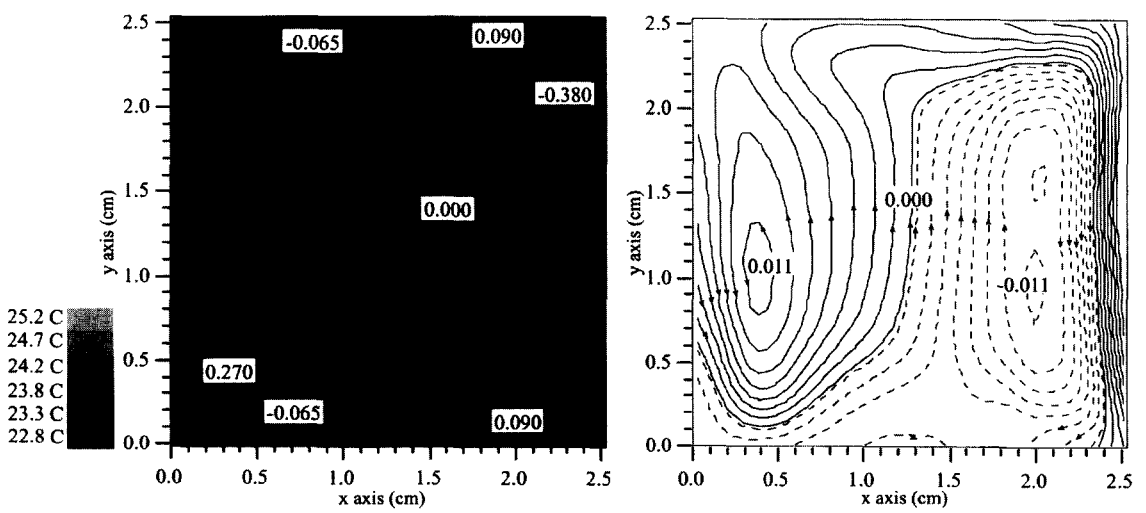

Figure 10. Position 1: 90° phase-shift. The right is the streamline plot, and the left is the vorticity plot superimposed over the temperature plot. The temperature, vorticity, and streamline contours are in increments of 0.485° centigrade, 0.045/s, and .0015 m^2/s, respectively. The axes are in centimeters.

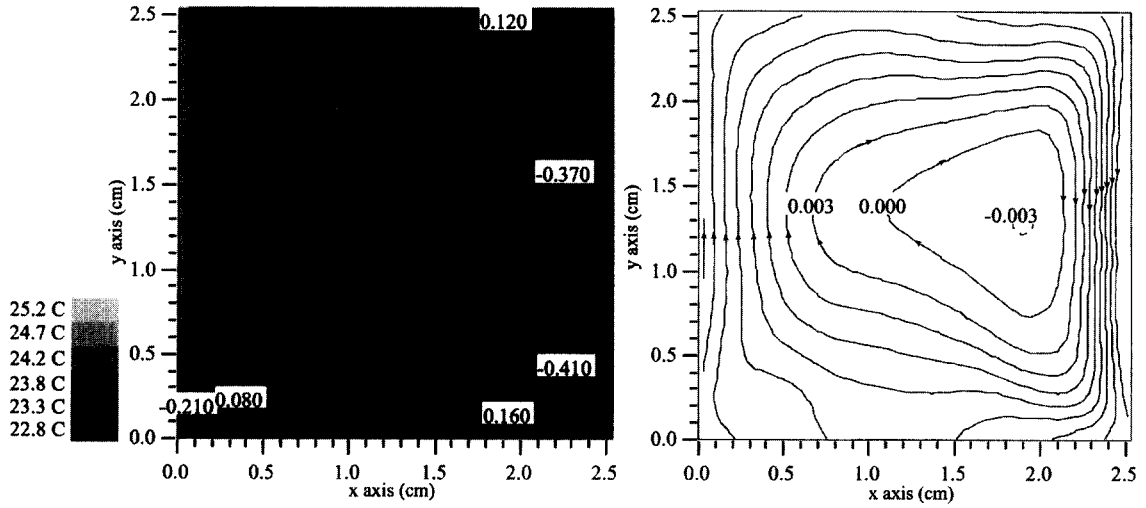

Figure 11. Position 2: 90° phase-shift. The right is the streamline plot, and the left is the vorticity plot superimposed over the temperature plot. The temperature, vorticity, and streamline contours are in increments of .485° centigrade, 0.04/s, and .003 m^2/s, respectively. The axes are in centimeters.

motions, it is evident that, at this stage, the development of the thermal boundary layer is mainly through conduction. Adjacent to the developing hot thermal boundary layer, remnants of the cold thermal boundary layer from the previous half cycle are seen toward the lower-left part of the cell. The vorticity distributions show that the previous cold thermal boundary layer, while moving downward under the buoyancy force, has also convected the vorticity generated through the previous half cycle. Also, the generation and diffusion of the negative vorticity is seen on the left sidewall. The forcing of the right sidewall, however, is 90° out of phase with the forcing on the left sidewall. The streamlines also show two side-by-side rollers, where the right roller is more dominant than the left roller. Thus, at this point, this position shows a situation where the flow is similar to the 0° phase-shift case, except that the adjacent rollers are not of equal strength.

The temperature field at this point shows a more developed, but cold, thermal boundary layer on the right sidewall. Because of this, as mentioned earlier, the flow has developed a higher velocity and momentum by the right sidewall. The vorticity field shows that the vorticity distribution along this sidewall is almost uniform. The core of the fluid is almost devoid of vorticity. The only vorticity that we see in this area is that which diffuses from the strong vorticity distribution along the right sidewall. Lastly, the streamlines show that the center plane at this position exhibits both two-dimensional and three-dimensional behavior. The flow on the right half of the cell is fully developed into a two-dimensional clockwise roller. The only three-dimensionality exhibited on the right half is on the horizontal walls, where the streamlines terminate on the walls. Yet the rotating flow in the left half of the cell is much weaker, owing to the smaller velocities from the

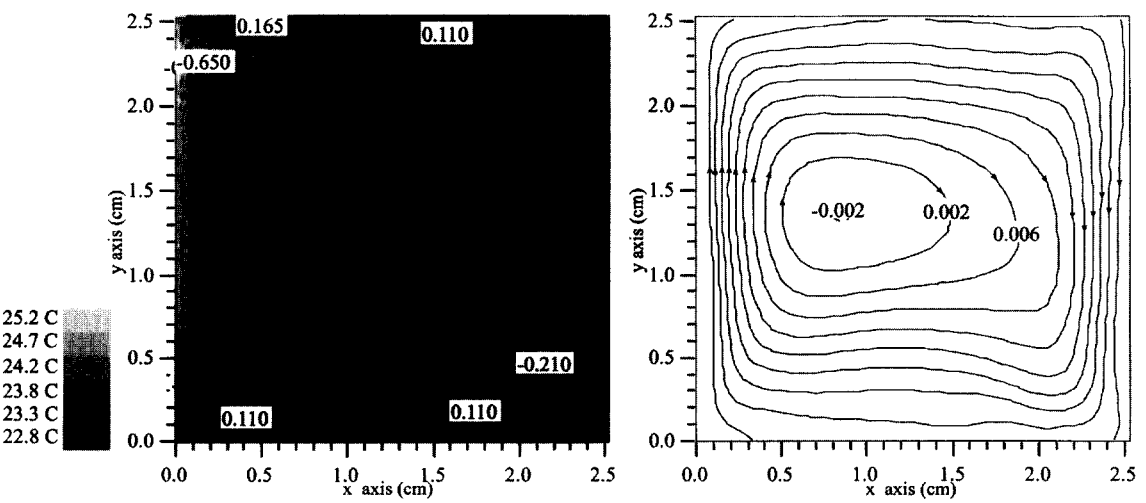

Figure 12. Position 4: 190° phase-shift. The right is the streamline plot, and the left is the vorticity plot superimposed over the temperature plot. The temperature, vorticity, and streamline contours are in increments of .485° centigrade, 0.04/s, and .004 m^2/s, respectively. The axes are in centimeters.

flow reversal on that side. This flow reversal shows a three-dimensional behavior, because the streamlines terminate onto the walls on the left-hand sides of the cell.

Position 2. The temperature field seen in Fig. 11 shows that the hot thermal boundary layer on the left sidewall has developed further. The vorticity distribution shows that the vorticity associated with the previous thermal boundary layer has disappeared. This can also be verified by the fact that the temperature variations that existed owing to the previous cold thermal boundary layer have now decreased to just a cold patch at the bottom-left corner of the cell. Note that the entrainment of the fluid from this cold patch into the hot thermal boundary layer has baroclinically generated vorticity, as can be seen in the vorticity that has grown with respect to the previous position. The thermal forcing on the right sidewall is now becoming evident as positive vorticity is being generated. This is evident from the positive vorticity near the right sidewall at position 1. At position 2, the right sidewall vorticity has increased and begun to diffuse slowly toward the core. As such, no more negative vorticity is being generated and all that was generated has begun to advect down the sidewall. After flowing down the right sidewall, the fluid turns the corner and moves toward the core of the fluid. In doing so, it begins the development of the intrusion layer. Note that the vorticity associated with it is positive. The triangularly shaped streamlines indicate that the flow along the right sidewall travels down the wall, around the corner, and up toward the core of the cell. The flow also travels from the core of the cell diagonally into the upper-right corner of the cell. This is also evident in the vorticity plots. The vorticity contours show that the zero vorticity line is diagonal, traveling from the core toward the upper-right corner of the cell and from the core to the lower-right corner of the cell. Note that the core is almost devoid of any vorticity. Also, in this position, the right heater is cooling, whereas the left heater is heating, thus producing a single roller, as can be seen in the streamline plot. Therefore, at this position, the flow resembles that seen in the 180° case. Notice that the left half shows weaker flow and a slightly more three-dimensional behavior with respect to the right half, where the flow is has higher velocities.

Position 4. The temperature field shown in Fig. 12 shows that the thermal boundary layer on the left sidewall has developed further and that the temperature within the intrusion layer has increased. This is because the thermal forcing on the left sidewall has started to increase even further with respect to the previous position. Owing to this forcing, negative vorticity is generated in the left wall. Notice that the newly developed, hot thermal boundary layer is entraining fluid from the lower-left corner, thus reducing the size of the cold spot located in that corner from the previous position. Also, the thermal forcing on the right sidewall is reducing with respect to the previous position. The cold layer on the right sidewall has now convected farther down and has developed into a cold patch in the lower-right corner. The vorticity plot shows that the distribution of vorticity on the right sidewall is not uniform anymore and that the center of the vorticity has shifted downward. This indicates that the cold thermal forcing on the wall is starting to reverse, as can be seen in Fig. 4c. Because the right wall's temperature is starting to reverse, no more negative vorticity is being generated, and thus the cold thermal boundary layer is no longer driven by the sidewall's forcing. Also, evidence of the temperature reversal on the right sidewall is seen in the creation of positive vorticity on the right sidewall. The cold layer associated with this negative vorticity has further advected downward under its buoyant force and has advected its vorticity as well. Also evident is the diffusion of the positive vorticity from the right sidewall inward toward the core. Also seen in the vorticity plots is the vorticity on the right side of the bottom wall, which is associated with the intrusion layer. Because the flow on the right sidewall is starting to reverse, the negative vorticity associated with the cold layer has decreased in magnitude. This is also true for the vorticity associated with the intrusion layer on the bottom wall. The development of the intrusion layer along the top wall, however, is showing signs of increasing its vorticity. The streamlines show that, at this point, the flow achieves its most two-dimensional behavior, because almost no streamlines terminate on the walls. Finally, within the core, the vorticity level is negligible with respect to the rest of the flow.

DISCUSSION

Similarities between the Time-Varying Experiments

After detailed study of the process of the flow behavior in the time-varying experiments, several features that were similar among them became evident. Perhaps the most evident is the development of the thermal boundary layers on the sidewalls. Regardless of the phase difference between the heating cycle of the heaters, each of the thermal boundary layers on the sidewalls developed and decayed independently of each other. Thus, the development of a hot thermal boundary layers is summarized as follows:

1. Initially, heat is conducted through a layer of fluid adjacent to the sidewall.
2. Upon convection of the thermal layer, vorticity is generated and diffused from the sidewall inward.
3. Also upon convection, the hot thermal boundary layer entrains colder fluid left over from the previous thermal boundary layer.
4. The thermal boundary layer approaches the top horizontal wall and turns around the corner.
5. As long as the sidewall is thermally forced, the vorticity along this wall will be generated. However, when the forcing starts to reverse, for a brief moment, the sidewalls will not be thermally forced, and vorticity will not be generated. At this point, the hot thermal layer will react to its buoyant force and move upward, convecting the vorticity within it as well.
6. Meanwhile, the cooling cycle begins at the sidewall, and this whole process repeats itself for the development of the cold thermal boundary layer.

Another feature that is similar to all three time-varying experiments is the fact that the intrusion layers thicken as seen by Ivey [5]. Again, this is most evident in the streamlines for the 180° phase-shift experiment that become elongated in opposite corners, thus simulating a rhomboid

appearance. A third feature found to be similar to all cases is that the core is devoid of vorticity for most of the cycle. This indicates that, when there is flow, it is irrotational. Almost all the vorticity is concentrated within the thermal boundary layers or within the intrusion layers. A last feature common to all cases is that the main features of the flow are seen within the same location within the heating and cooling cycle. These happen to be at two locations: (1) when the heaters are fully heating or cooling; and (2) when the heater's are almost in midway transition between full heating and full cooling.

Differences between the Time-Varying Experiments

Perhaps the most obvious difference in the three time-varying experiments is the number of rotating cells created within the cavity. In the 0° phase-shift experiment, each half cycle produces two rotating cells symmetrically located side by side about the y axis. The directions of rotation of these cells changed every half cycle. In the 180° phase-shift experiment, each half cycle produced one rotating cell. The direction of rotation of this cell changed from clockwise to counterclockwise every half cycle. Finally, in the 90° phase-shift experiment, there are both one cell and two cell developments within the cavity. If the phase of the heaters is such that they are out of phase, one cell forms. However, as the phase shift changes such that both heaters either heat or cool, two cells develop within the cavity.

The second difference concerns the vorticity within the core of the cavity. The only time at which the core of the cavity is not devoid of vorticity for the 0° and 180° phase-shift experiments is when the flow has almost zero velocity throughout the domain and is ready to reverse. In the 90° phase-shift experiment, the only time at which the core is not devoid of vorticity is when the velocity adjacent to one of the sidewalls is zero. In the 0° phase-shift experiment, at position 1, the vorticity field is seen to be symmetric about the center vertical axis of the cell. For the 180° phase-shift experiment, however, the flow at position 8 shows that the vorticity distribution is symmetric about the center of the cell. In the 90° phase-shift experiment, the flow shows characteristics of both the 180° and the 0° phase-shift cases. In Fig. 10, where there are two rollers within the cell, there is vorticity being generated at the right sidewall, whereas none is being generated at the left sidewall. In Fig. 11, though there is only one roller within the cell, the flow is being driven by the right sidewall. This generates vorticity at that wall. However, because the flow is not being driven at the left sidewall, there is no vorticity developed at that wall.

The development of the intrusion layers will differ depending on the phase of the heaters. In the 180° phase-shift case, because each sidewall is developing an intrusion layer on either the top or the bottom wall, the intrusion layers will grow and span across most of the length of the horizontal walls. But in the 0° phase-shift experiment, both sidewalls are developing an intrusion layer on the same horizontal wall. Thus, the intrusion layers meet and interfere with each other at the midpoint of the horizontal wall. In the 90° phase-shift experiment, the behaviors of both the 0° and the 180° phase-shift experiment are seen. When the heaters are in phase and are both heating or cooling, intrusion layers are created by both thermal boundary layers that interfere on the horizontal wall, as in the 0° phase-shift experiment. However, once one of the wall's forcing gets stronger while the other becomes weaker; the intrusion layer, owing to the strong forcing, overtakes the weaker one and spreads over most of the length of the horizontal wall.

Comparison of Time-Varying Flow with Steady-State Case

Comparison with the steady state shows some interesting results. In the steady state, the core remains stationary, allowing the vertical stratification to develop. However, in the time-varying experiments, the vertical thermal stratification is weaker. For the steady-state case, because the sidewalls are continuing to force the flow, the vorticity distribution along the sidewalls remains uniform along the walls' length. However, in the time-varying flows, because the forcing is continually changing, the vorticity distribution along the wall is always changing as well. Lastly, the core of the fluid in the steady-state case remains stationary, whereas the core in the oscillatory cases is continually in motion. This is directly responsible for the mixing within the cell, as is apparent from the many thermal "islands" in the sinusoidally forced cases.

The Two- and Three-Dimensionality of This Flow

Perhaps most interesting in this flow is that it exhibits both two- and three-dimensional behavior within the midplane of the cavity. For the steady-state case, the streamlines show complete two-dimensionality. Within the center of this plane, it is seen that the 0.0 streamline is slightly pinched, indicating the possible existence of the double spiral seen by Hiller *et al.* [7, 8]. Once again, the results of Hiller *et al.* show the existence of these streamline spirals extending from the sidewalls to the center plane. However, their results also show that the majority of the streamlines are located within the center plane and that, if a particle were released into this spiral, it would spend more time in the center plane than it would in the rest of the flow. This could explain why the center plane exhibits two-dimensionality while the rest of the flow does not.

This phenomena is also seen in all three oscillatory cases. For each position of the heating cycle within each of the three cases where the flow has achieved full heating/cooling, and therefore higher velocities, the streamlines exhibit two-dimensional behavior for aforementioned reasons. However, for the positions within the heating cycle within each of the three cases where the flow is just reversing its heating/cooling, and the velocities are small, the streamlines exhibit three-dimensional behavior. We believe that this is due to the fact that the flow reversal is rearranging the spiral streamlines seen by Hiller *et al.*, thereby generating the three-dimensionality seen with the center plane.

PRACTICAL SIGNIFICANCE

The simultaneous measurement of temperature and velocity is critical for understanding and improving the designs for mixers, heat exchangers, and so forth, where heat transfer is crucial. The present paper demonstrates the DPITV technique and applies this technique to mapping

the flow required within a cubic cavity. Comparison of the oscillatory cases with the steady case shows that the oscillatory cases have many thermal islands within the fluid, indicating mixing, whereas the steady-state case shows few thermal islands and therefore almost no mixing.

CONCLUSIONS AND RECOMMENDATIONS

In conclusion, a technique that is capable of measuring temperature and velocity simultaneously is successfully applied to study flow within a forced convection cell. The forcing is created by the sinusoidal heating and cooling of the two opposing sidewalls at 0°, 180°, and 90° phase-shifts. In summary, it is seen that, in the steady-state case, the flow is confined to the boundaries of the cell, whereas the core remains stationary, which allows for the development of a vertical stratification within the core. Owing to steady heating/cooling, the thermal boundary layers and intrusion layers are fully developed. The distribution of vorticity is mostly on the sidewalls, as the core remains devoid of vorticity. In the time-varying flow, the generation of the vorticity field is seen on the sidewalls as well as in its distribution in the intrusion layers and the core. It is seen that, for all the time-varying flows, the vertical gradient is shallower than that developed in the steady state experiment. Lastly, and perhaps most interesting, is that the oscillatory cases produce many thermal "islands," indicating mixing is occurring.

Therefore, by the qualitative analysis of the streamline, vorticity, and temperature fields, the basic flow phenomena associated with the steady and sinusoidally forced flows within a square convection cell have been determined and explained. However, this work raises several questions. For example, how much is the mixing enhanced in the time-varying experiment compared with the steady-state case? Would the mixing be more efficient if each of the heaters were heated at different frequency ratios? To answer these questions, it is first necessary to develop the DPITV technique further so that the errors associated with it can be reduced. This will then allow measurable quantities such as the heat flux, q'', turbulent heat fluxes, such as $u'T'$, and turbulent shear stresses, such as $u'v'$, which are essential to the study of mixing. Only then will detailed and qualitative flow analysis provide useful and convincing answers to these questions.

We would like to gratefully acknowledge the financial support of DARPA/URI Program Contract No. N00014-86-K-0748 and the NSF Division of Thermal Transport and Thermal Processes (CTS-941-8973).

NOMENCLATURE

- A aspect Ratio, dimensionless
- g gravitational Acceleration, m/s^2
- p pressure (hydrostatic), N/m^2
- q'' heat flux, W/m^2
- Ra Rayleigh number, dimensionless
- T temperature, centigrade
- ΔT temperature difference, centigrade
- u x-direction velocity, cm/s
- v y-direction velocity, cm/s
- x horizontal axis, cm
- y vertical axis, cm
- a coefficient of thermal expansion, centigrade^{-1}
- v kinematic viscosity, m^2/s

Greek Symbols

- ρ density, Kg/m^3
- σ Prandtl Number, dimensionless
- ω vorticity, s^{-1}

REFERENCES

1. Bachelor, G. K., Heat Transfer by Free Convection across a Closed Cavity between Vertical Boundaries at Different Temperatures, *Q. J. Appl. Math.* **12**, 209–233, 1954.
2. Gill, A. E., The Boundary Layer Regime for Convection in a Rectangular Cavity, *J. Fluid Mech.* **26**, 515–536, 1966.
3. Eckert, E. R. G., and Carlson, W. O., Natural Convection in an Air Layer Enclosed between Two Vertical Plates with Different Temperatures, *Int. J. Heat Mass Transfer* **2**, 106–120, 1961.
4. Patterson, J. C., and Imberger, J., Unsteady Natural Convection in a Rectangular Cavity, *J. Fluid Mech.* **100**, 65–86, 1980.
5. Ivey, G. N., Experiments on Transient Natural Convection in a Cavity, *J. Fluid Mech.* **144**, 389–401, 1984.
6. Schladow, S. G., Patterson, J. C., and Street, R. L., Transient Flow in a Side-Heated Cavity at High Rayleigh Number: A Numerical Study, *J. Fluid Mech.* **200**, 121–148, 1989.
7. Hiller W. J., Koch, St., and Kowalewski, T. A., Three-Dimensional Structures in Laminar Natural Convection in a Cube Enclosure, *Exp. Thermal Fluid Sci.* **2**, 34–44, 1989
8. Hiller W. J., Koch St., Kowalewski, T. A., De Vahl Davis, G., and Behnai, M., Experimental and Numerical Investigation of Natural Convection in a Cube with Two Heated Side Walls, *Proceedings of the IUTAM Symposium: Topological Fluid Mechanics*, H. K. Moffat, and A. Tsinober, Eds., pp. 717–729, August 13–18, 1989.
9. Patterson, J. C., and Armfield, S. W., Transient Features of Natural Convection in a Cavity, *J. Fluid Mech.* **219**, 469–497, 1990.
10. Schladow, S. G., Oscillatory Motion in a Side-Heated Cavity, *J. Fluid Mech.* **213**, 589–610, 1990.
11. Tong, W., and Koster, J., Natural Convection of Water in a Rectangular Cavity Including Density Inversion, *Int. J. Heat Fluid Flow* **14**(4), 336–375, 1993.
12. Dabiri, D., The Effects of Forced Boundary Conditions on the Flow Field of a Square Cavity, Ph.D. Thesis, Applied Mech. Eng. Sci., Univ. California at San Diego, San Diego, California, 1992.
13. Dabiri, D., and Gharib, M., Digital Particle Image Thermometry: The Method and Implementation, *Exp. Fluids* **11**, 77–86, 1991.
14. Willert, C. E., and Gharib, M., Digital Particle Image Thermometry, *Exp. Fluids* **10**, 181–193, 1991.
15. Kimura, I., Takamori, T., Ozawa, M., Takenaka, N., and Manabe, Y., Quantitative Thermal Flow Visualizations Using Color Image Processing: Application to a Natural Convection Visualized by Liquid Crystals, *Flow Visualization*, B. Khaloghi, M. J. Braun, and C. J. Freitas, Eds., ASME FED-Vol. 85, 69–76, 1989.
16. Ozawa, M., Muller, U., Kimura, I., and Takamori, T., Flow And Temperature Measurement of Natural Convection in a Hele-Shaw Cell Using a Thermo-Sensitive Liquid-Crystal Tracer, *Exp. Fluids* **12**, 213–222, 1992.

Received April 1, 1996; revised August 23, 1996